Check for updates

Re-detection and a possible time variation of soft X-ray polarization from the Crab

Hua Feng [1,2 ✉], Hong Li[2], Xiangyun Long[2], Ronaldo Bellazzini[3], Enrico Costa[4], Qiong Wu[2], Jiahui Huang[2], Weichun Jiang[5], Massimo Minuti[3], Weihua Wang[6], Renxin Xu[6], Dongxin Yang[2], Luca Baldini[3], Saverio Citraro[3], Hikmat Nasimi[3], Paolo Soffitta[4], Fabio Muleri[4], Aera Jung[2], Jiandong Yu[7], Ge Jin[8], Ming Zeng [2], Peng An[7], Alessandro Brez[3], Luca Latronico[9], Carmelo Sgro [3], Gloria Spandre[3] and Michele Pinchera [3]

The Crab nebula is so far the only celestial object with a statistically significant detection in soft X-ray polarimetry[1-4], a window that has not been explored in astronomy since the 1970s. However, soft X-ray polarimetry is expected to be a sensitive probe of magnetic fields in high-energy astrophysical objects, including rotation-powered pulsars[5-7] and pulsar wind nebulae[8]. Here we report the re-detection of soft X-ray polarization after 40 years from the Crab nebula and pulsar with PolarLight[9], a miniature polarimeter utilizing a novel technique[10,11] onboard a CubeSat. The polarization fraction of the Crab in the on-pulse phases was observed to decrease after a glitch of the Crab pulsar on 23 July 2019, while that of the pure nebular emission remained constant within uncertainty. The phenomenon may have lasted about 100 days. If the association between the glitch and polarization change can be confirmed with future observations, it will place strong constraints on the physical mechanism of the high-energy emission[12-14] and glitch[15-17] of pulsars.

In the energy band of a few kiloelectronvolts (hereafter referred to as the soft X-ray band), where the emission of most high-energy astrophysical objects peaks, X-ray polarimetry is argued to be a powerful and sometimes unique tool in diagnosing the magnetic field, geometry and emission mechanism in astrophysics[18,19]. However, owing to technical difficulties, soft X-ray polarimetry has been a practically unexploited field, with so far the only detection taking place in the 1970s[1-3]. In 2001, high-sensitivity soft X-ray polarimetry became possible with the invention of photoelectric polarimeters[10,11].

A polarimeter onboard a CubeSat, named PolarLight[9], was launched into a Sun-synchronous orbit on 29 October 2018, as the first flight test of the new technique. PolarLight is a gas pixel detector capable of measuring X-ray polarization via electron tracking. The instrument has a collecting area of only $1.6\,cm^2$, with a collimator to constrain the field of view to 2.3° (full-width at half-maximum). Therefore, PolarLight can be treated as a miniature X-ray polarimeter built on the basis of a high-sensitivity technique[20].

Since launch, the Crab (here referring to both the nebula and pulsar if not specified) has been the primary target of PolarLight and routinely observed, except from early May to early July when the source was too close to the Sun on the sky plane. Here we report

the results from observations as of early December 2019, with a total exposure of about 660 ks for the Crab and 165 ks for the background. Given the Crab spectrum, the polarization measurement is most sensitive in the energy range of 3.0–4.5 keV. The background mainly results from charged particles, and some of them can be discriminated by charge morphology. In the 3.0–4.5 keV energy range, valid events that can be used for polarimetry have a mean count rate of about 0.03 counts per second when observing the Crab, with an average background contamination of about 10%. The polarization fraction (PF) and polarization angle (PA) are calculated on the basis of the Stokes parameters[21]. We adopt the Bayesian approach to perform the point and interval estimates of the intrinsic polarization. Details about the data reduction and analysis can be found in Methods.

In the 1970s, the Bragg polarimeter onboard the Eighth Orbiting Solar Observatory (OSO-8) measured X-ray polarization of the Crab at two narrow bands around 2.6 keV and 5.2 keV, respectively[2,3]. At 2.6 keV, the total Crab emission has $PF = 0.157 \pm 0.015$ and $PA = 161.1° \pm 2.8°$, and the pulsar-free nebular emission has $PF = 0.192 \pm 0.010$ and $PA = 156.4° \pm 1.4°$. The results at 5.2 keV are consistent with those at 2.6 keV within errors.

Time-averaged polarization measurements of the Crab with PolarLight, using all of the data in the energy range of 3.0–4.5 keV, are shown in Fig. 1a. The result suggests that the Crab emission in this energy band has an average PF of $0.153^{+0.031}_{-0.030}$ and an average PA of $145.8° \pm 5.7°$, detected at a significance level of 4.7σ. Our PF is consistent with that obtained with OSO-8, while the PA differs by approximately 2σ. For comparison with the OSO-8 results, the polarization of the pulsar-free nebular emission is shown in Fig. 1b, calculated from the off-pulse phase interval (Extended Data Fig. 3), which is in line with the definition used in the OSO-8 analysis. Our off-pulse result has a relatively large uncertainty and is consistent with that from OSO-8. On 23 July 2019, a glitch was detected in the Crab pulsar[22]. To investigate the possible phase and time dependence of polarization, we analyse the data in two phase ranges (on-pulse and off-pulse) and two epochs (before and after the glitch), respectively. The results are listed in Table 1.

The most interesting finding is that a time variation of polarization is detected for emission during the on-pulse phases. The PF is found to decrease from $0.288^{+0.071}_{-0.073}$ before the glitch to $0.101^{+0.047}_{-0.051}$

[1]Department of Astronomy, Tsinghua University, Beijing, China. [2]Department of Engineering Physics, Tsinghua University, Beijing, China. [3]INFN-Pisa, Pisa, Italy. [4]IAPS/INAF, Rome, Italy. [5]Key Laboratory for Particle Astrophysics, Institute of High Energy Physics, Chinese Academy of Sciences, Beijing, China. [6]Department of Astronomy, School of Physics, Peking University, Beijing, China. [7]School of Electronic and Information Engineering, Ningbo University of Technology, Ningbo, China. [8]North Night Vision Technology Co. Ltd, Nanjing, China. [9]INFN, Sezione di Torino, Torino, Italy. ✉e-mail: hfeng@tsinghua.edu.cn
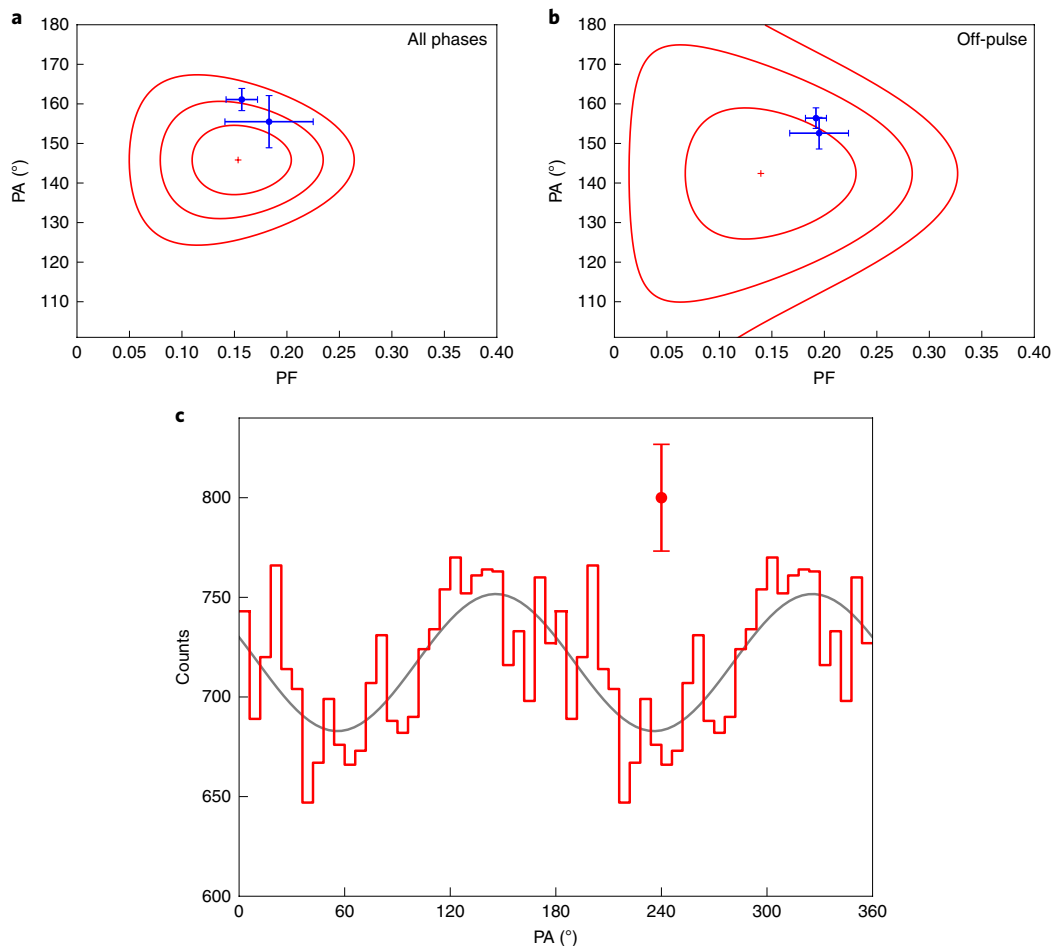
Fig. 1 | Polarization measurements of the Crab with PolarLight. a,b, Bayesian posterior distribution of PF and PA derived from PolarLight observations of the Crab in the energy range of 3.0–4.5 keV, for data in all phases (**a**) and data in the off-pulse phases that include pulsar-free nebular emission (**b**). The red plus indicates the point estimate and the contours encircle the 1σ, 2σ and 3σ credible intervals. The blue points and error bars mark the Crab polarization measured with the polarimeter on OSO-8 at 2.6 keV (one with smaller errors) and 5.2 keV (one with larger errors)[2,3]. **c,** A modulation curve (red) using data in all phases against the model (grey) inferred in this Letter (see parameters in Table 1) is provided for visual inspection. The error bar indicates the typical 1σ error of the counts in each phase bin.

after the glitch. We divide the data into smaller time bins and calculate polarizations in the on-pulse and off-pulse phases, respectively (Fig. 2). The on-pulse polarization exhibited an abrupt change after the glitch, while the off-pulse polarization remained constant. The Bayes factor is adopted to test the significance of a constant PF against a PF decrease over different time intervals after the glitch (Methods). A PF decrease after the glitch is favoured with strong evidence using data after 30–100 d of the glitch (Fig. 3). Within ~30 d after the glitch, the statistic is not high enough to claim any statement. After ~100 d of the glitch, the PF started to recover leading to weaker evidence, which is consistent with the polarization lightcurve shown in Fig. 2. A change (either decrease or increase) in PF after the glitch is found to have substantial evidence, also shown in Fig. 3. As an independent test, the posterior distribution of polarization derived from data before the glitch is compared with that within 100 d after the glitch (Methods). The two measurements are not consistent with each other at a 3σ level, suggesting that the above conclusion is valid. In addition, a bootstrap test produces a consistent result that the decrease is evident at a significance of 3σ (Methods). We emphasize that the choice of 100 d after the glitch is not subjective; choosing any time from 30–100 d after the glitch results in the same conclusion, as shown in Fig. 3.

The rate of directly measured background, as well as the rate of events rejected by particle discrimination, is found to be constant on timescales longer than the orbital period (Methods). No polarization modulation in background is detected. Taking into account the upper limit of polarization and flux contribution, the background is unable to account for the observed change in the PF (Methods). The contribution of background is the same to both on-pulse and off-pulse results. Thus, the variation can not be a result of change in background. The instrumental systematic error on the PF is below 1% (Methods). Laboratory tests indicate that the modulation factor varies no more than 4% in response to the change of gain (Methods). The uncertainty of the modulation factor due to inaccurate gain calibration is less than 5% (Methods). Similarly, a change in the modulation factor will affect results in all phases and can be ruled out. To conclude, we claim strong evidence for a decrease in PF after the glitch of the Crab pulsar, and rule out the possibility that this is due to background or calibration systematics.

The results suggest that the variation is more likely associated with the pulsar, because it is more significant in the on-pulse phases. The pulsar occupies roughly 7–8% of the total Crab emission in the energy band of 3.0–4.5 keV (ref. [23]) or ~12% in our on-pulse phase interval. Such a flux fraction is possible to produce the observed

Table 1 | Phase- and time-dependent polarization measurements of the Crab with PolarLight in the energy range of 3.0–4.5 keV

Phase[a]	Epoch[b]	PF	PA (°)
All	All	$0.153^{+0.031}_{-0.030}$	145.8 ± 5.7
Off-pulse	All	$0.140^{+0.052}_{-0.054}$	142.4 ± 11.0
On-pulse	All	$0.158^{+0.039}_{-0.039}$	147.6 ± 7.0
All	Before glitch	$0.243^{+0.057}_{-0.057}$	144.5 ± 6.7
All	After glitch	$0.113^{+0.037}_{-0.038}$	146.9 ± 9.6
Off-pulse	Before glitch	$0.137^{+0.076}_{-0.110}$	149.9 ± 21.0
Off-pulse	After glitch	$0.127^{+0.061}_{-0.067}$	138.7 ± 15.1
On-pulse	Before glitch	$0.288^{+0.071}_{-0.073}$	142.7 ± 7.2
On-pulse	After glitch	$0.101^{+0.047}_{-0.051}$	153.0 ± 14.4

[a]For emission in all phases, the on-pulse phase interval that contains both pulsar and nebula emission, or the off-pulse interval that is free of pulsar emission. See Methods for definition. [b]Data in all times, before or after the Crab glitch on 23 July 2019. Errors are quoted as 68% credible intervals.

variation only if the pulsar PF is high. In that case, the observed PF decrease could be due to a large PA variation from the pulsar emission after the glitch. We try to estimate the pure pulsar polarization by subtracting the off-pulse polarization from on-pulse signals. However, no useful constraint can be made with the current data. A high degree of polarization during the on-pulse phases challenges nearly all of the pulsar emission models, which predict either a swing of PA with phases that leads to a low PF on average or a considerably low PF during the on-pulse phases[5–7]. A change of the nebular polarization is another possibility, which cannot be ruled out by the currently available data.

Glitches are thought to be a result of catastrophic superfluid vortex unpinning[15–17]. In the vortex model, the sudden angular momentum transfer between the faster-rotating superfluid interior and the crust results in an abrupt spin-up. The motion of the core superfluid vortices may alter the core magnetic flux tubes[24]. The sudden

spin-up of the crust may cause a change in the configuration of magnetic fields threaded in it, and consequently in the co-rotating magnetosphere. For Crab-like young pulsars, starquakes may trigger the glitch[17] and lead to a natural change in the magnetosphere, especially if the crust cracks in the polar region. The timescale of the polarization variation that we observed here (tens of days) for the Crab is much longer than that in the radio band observed in the Vela pulsar (a few seconds)[25], but is consistent with the post-glitch recovery timescale of the Crab pulsar[26]. For rotation-powered pulsars, the emission regions of X-rays and radio may be different[12–14]. The mechanism that drives the glitches could also be different for Vela and Crab[27]. As X-rays can be emitted in a large range of altitudes all the way from regions close to the surface to the light cylinder or even beyond, it is very likely that a small change in the magnetosphere could result in a large change in the observed PA via the leverage effect.

This experiment demonstrates that a CubeSat with a tiny detector for a dedicated science goal can yield valuable data. Such space projects with a relatively low cost and short duration are also ideal platforms for student training. The successful operation of PolarLight indicates that the window of X-ray polarimetry in the few kiloelectronvolts energy range has been re-opened after 40 years. Future missions such as the Imaging X-ray Polarimetry Explorer (IXPE)[28] and enhanced X-ray Timing and Polarimetry (eXTP)[29] will have a much higher sensitivity and can perform in-depth studies of this topic.

Methods

Observations. PolarLight flies in a high-inclination low-Earth orbit, where the charged particle flux is high in the two polar regions and the South Atlantic anomaly region. The high-voltage power supply of the detector needs be powered off in these regions. Taking into account the Earth occultation and other constraints (for example, by the star tracker), the total duration in a day that the target is observable is roughly 200 min. We note that some orbits are not used if the continuous observable time is not long enough to power on and off the high-voltage power supply. The first observation of the Crab took place on 1 March 2019. About one month later, regular observations could be scheduled in an efficient way. The Crab has been observed routinely since then. From 11 May to 10 July in 2019, no observation was scheduled for the Crab because the source was close to the Sun on the sky plane. In this Letter, observations as of 3 December
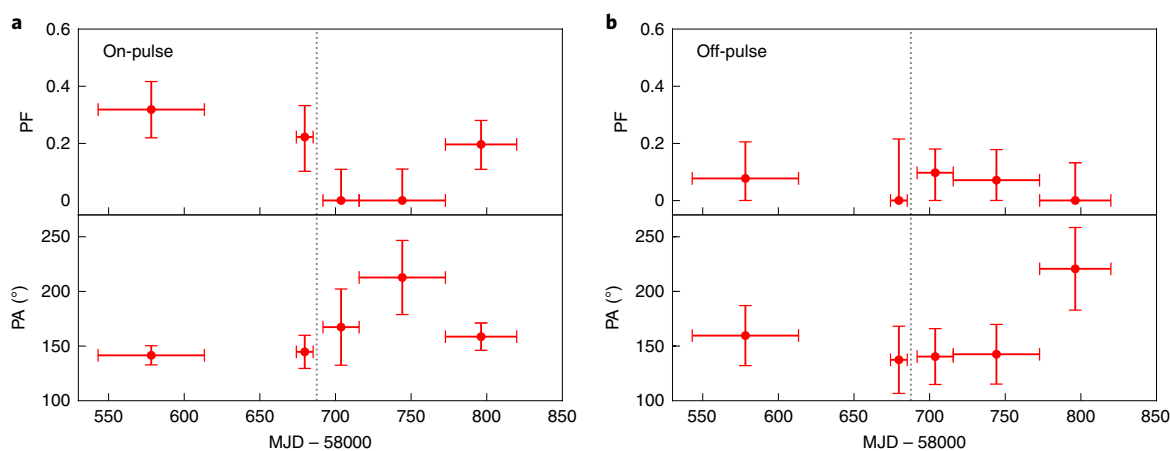

Fig. 2 | Time dependent polarization of the Crab. a,b, The Crab X-ray polarization in the 3.0–4.5 keV band as a function of time, respectively, for events in on-pulse phases (**a**) and off-pulse phases (**b**). The first bin includes all observations in the first observing window (May 2019 and before). As observations could not be scheduled efficiently in that epoch, it spans over a large time interval. The second bin includes observations in the second window (July 2019 and after) but before the Crab glitch on 23 July 2019, marked by a vertical dotted line. The following bins are from the rest observations in the second window equally divided by the number of photons. The net effective exposure in each bin is 90, 98, 168, 158 and 145 ks, respectively. The horizontal bar indicates the time span of the measurements. The vertical error bar indicates the 68% credible interval of PF or PA. We note that PA is wrapped between 0° and 180° by definition, but to avoid a visual impression for a large PA variation, here we have mapped some PAs around 30–40° to 210–220°. The on-pulse polarization is observed to vary after the pulsar glitch, while the nebular polarization remains constant. MJD, modified Julian date.
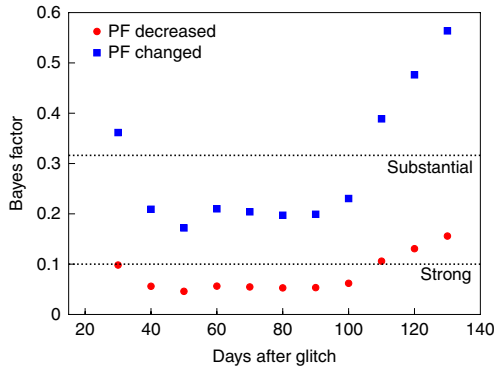
Fig. 3 | Significance test for a polarization variation associated with the glitch. Bayes factor to test the model ($\mathcal{M}_0$) that the PF remained constant against the model ($\mathcal{M}_1$) that there was a decrease (red) or change (blue; either decrease or increase) in PF after the glitch. As the variation may be a one-time transient behaviour, the test is done with data until some days after the glitch, which is indicated as the x axis. If the Bayes factor is lower than $10^{-1/2}$, the evidence against $\mathcal{M}_0$ is regarded as substantial; if it is lower than 10^{-1}, the evidence against M_0 is strong[30]. The results suggest that there is strong evidence that the PF decreased after the glitch and lasted about 100 d, or substantial evidence that there was a change (either decrease or increase) after the glitch.

2019 are included. After that date, there were several major upgrades of the onboard computer and science observations were paused for a while.

Gain calibration. The detector gain is calibrated by comparing a simulated Crab spectrum[31], an absorbed power-law spectrum with an absorption column density of 4.5×10^{21} cm^{-2} and a photon index of 2.07, with the observed pulse height spectrum. The background spectra are obtained via observations of the blank sky and Earth atmosphere. The two background spectra show no difference as charged particles are the main cause of the background, which is confirmed by simulations. The pulse height spectrum of the background can be described by an exponentially cutoff power-law function, with parameters found from pure background observations. In the energy calibration, we fit the observed spectrum during Crab observations with the sum of the two components, with the spectral shapes fixed but the normalizations and pulse height to energy relation as free parameters. Because the two components dominate at different energy ranges (Extended Data Fig. 1), they can be readily decoupled. With the gain calibrated in such a way, the peak position of the energy spectrum at different epochs has a mean of 2.16 keV with a standard deviation of 0.012 keV, suggesting that the uncertainty for the gain calibration is on the level of 1%. The track eccentricity is a function of energy, and its distribution in 3.0–4.5 keV shows a consistent shape with time, allowing us to constrain the gain uncertainty to be better than 5%. Even taking the more conservative estimate, the gain uncertainty will have no effect on the accuracy of the results.

Data reduction. The science data for each event include the arrival time and track image. With the track image, the photon energy and emission angle of the photoelectron on the detector plane can be inferred. Charged particles will also deposit energies in the detector, but usually leave a long, straight track behind, with multiple charge islands. To distinguish them, we select X-ray events if the image has a diagonal of no more than 70 pixels, an eccentricity not higher than 50 and only one isolated charge island. This step is called particle discrimination. Events near the edge of the detector (outside the central 14 mm × 14 mm region) are not used as they may have a partial deposit of charges. Then, to remove spurious modulation at a period of 60° due to the hexagonal pixels[32], we discard events with charges spreading on less than 58 pixels in polarization analysis. The choices of these criteria and parameters are justified by simulations and laboratory tests at 3.74 keV using 45° diffraction with the Al crystal. Given the modulation factor μ, measured counts from the Crab N and background fraction f_b, we calculate the quality factor $\left[\equiv \mu \sqrt{N}(1 - f_b) \right]$ of the detector as a function of energy in Extended Data Fig. 2. The quality factor is an indicator of the sensitivity of polarimetry. As one can see, 3.0–4.5 keV is the most sensitive energy range for polarimetry of the Crab. Inclusion of data down to 2 keV or up to 5 keV does not improve the polarimetric signal-to-noise ratio. In the energy range of 3.0–4.5 keV, the average modulation factor[9] is 0.35, and the background flux fraction is 10%.

Phase definition. The photon arrival time is converted to the Solar System barycentre using the Jet Propulsion Laboratory DE430 ephemeris[33]. The Jodrell Bank ephemeris for the Crab pulsar[34] is used to fold the pulse profile, shown

in Extended Data Fig. 3. To be in line with the definition used for the OSO-8 analysis[4], the phase interval from 17 ms to 30 ms after the primary pulse peak is defined as the off-pulse interval, while the rest is defined as the on-pulse interval. In our case, the on-pulse interval corresponds to a phase range from 0 to 0.62.

Polarization measurement. The polarization is calculated based on the Stokes parameters[21,35]. Here we use the subscript 'r' to denote reconstructed values and subscript '0' to denote intrinsic values. Given the position angle (ϕ) of each photoelectron, the source and background counts (S and B), and the average modulation factor (μ) in the energy band, the normalized Stokes parameters are

$$Q_r = \frac{1}{S} \sum_{i=1}^{S+B} \cos(2\phi_i) \tag{1}$$

$$U_r = \frac{1}{S} \sum_{i=1}^{S+B} \sin(2\phi_i) \tag{2}$$

The reconstructed PF (p_r) and PA (ψ_r) are

$$p_r = \frac{2}{\mu} \sqrt{Q_r^2 + U_r^2} \tag{3}$$

$$\psi_r = \frac{1}{2} \arctan \frac{U_r}{Q_r} \tag{4}$$

Owing to the positive-definite nature of polarization measurement, the estimate of PF will introduce a bias. The situation is worse towards low statistics, for example, when one tries to divide the data into smaller time or phase bins. The bias could be corrected by using the Bayesian approach[35,36], which is adopted to estimate the intrinsic parameters in this work. The prior distribution of p_0 is assumed to be uniform between 0 and 1, and that of ψ_0 is assumed to be uniform between 0 and π. The probability of measuring p_r and ψ_r given the intrinsic p_0 and ψ_0 is

$$\rho(p_r, \psi_r | p_0, \psi_0) = \frac{p_r}{\pi \sigma^2} \exp\left(-\frac{p_r^2 + p_0^2 - 2p_r p_0 \cos(2\psi_r - 2\psi_0)}{2\sigma^2}\right) \tag{5}$$

where $\sigma = \sqrt{2(S+B)}/(\mu S)$. The posterior distribution is written as

$$\rho(p_0, \psi_0 | p_r, \psi_r) = \frac{\rho(p_0, \psi_0)\rho(p_r, \psi_r | p_0, \psi_0)}{\iint \rho(p_0, \psi_0)\rho(p_r, \psi_r | p_0, \psi_0) \mathrm{d}p_0 \mathrm{d}\psi_0} \tag{6}$$

To estimate p_0 and ψ_0, we use the marginalized posterior distributions. For p_0, the maximum a posteriori of the marginalized posterior distribution is adopted for point estimate. ψ_r is an unbiased estimate of ψ_0 and is adopted for point estimate directly. The credible interval (the region of the highest posterior density) from the marginalized posterior distribution given a probability (68% or 90%; always specified in the text) is quoted as the error range. We note that the credible interval is non-symmetric for p_0 due to the nature of Rice distribution, but symmetric for ψ_0 (ref. [36]).

Test of a decrease/change in PF with the Bayes factor. Two models are defined, with $\mathcal{M}_0$ referring to a constant PF and $\mathcal{M}_1$ referring to a PF decrease after the glitch. The Bayes factor $\mathrm{BF}_{01}, = P(\mathcal{D}|\mathcal{M}_0)/P(\mathcal{D}|\mathcal{M}_1)$, is calculated to quantify how much $\mathcal{M}_0$ is favoured over $\mathcal{M}_1$ from the data $\mathcal{D}$. The likelihood is calculated using Monte-Carlo integration[37] as

$$P(\mathcal{D}|\mathcal{M}_i) \approx \frac{1}{N} \sum_{j=1}^{N} P(\mathcal{D}|\theta_j, \mathcal{M}_i) \quad (i = 0, 1) \tag{7}$$

where θ is the assembly of model parameters that follow $P(\theta|M_i)$, and N is the Monte-Carlo sample size and should be sufficiently large. The data include all the observations before the glitch and those within a certain range of days after the glitch. θ includes two intrinsic PFs, $p_{0,a}$ before and $p_{0,b}$ after the glitch, with $p_{0,a} = p_{0,b}$ for $\mathcal{M}_0$ and $p_{0,a} > p_{0,b}$ for $\mathcal{M}_1$. They are randomly sampled from the allowed parameter space. Then, with S and B in the two epochs and μ, the probability of data given the parameters can be computed as

$$P(\mathcal{D}|\theta, \mathcal{M}) = P(p_{r,a}|p_{0,a})P(p_{r,b}|p_{0,b}) \tag{8}$$

where $P(p_r|p_0)$ is the likelihood of p_r given p_0, a Rice distribution that can be obtained by integrating equation (5) over ψ. In the case to test against a change (either increase or decrease) in PF after the glitch, one simply needs to modify $\mathcal{M}_1$ to have two independent intrinsic PFs, $p_{0,a}$ and $p_{0,b}$, respectively, before and after the glitch.

Other evidence for a decrease in polarization after the glitch. Here we compare two samples. Sample A contains data before the glitch and sample B contains data within 100 d after the glitch. The end date of 100 d after the glitch is not a subjective choice; the same conclusion remains if one chooses any date from ~30 d to ~100 d after the glitch (Fig. 3). The posterior distributions of polarization with the two

samples are plotted in Extended Data Fig. 4. Each measurement is not consistent with the other at a 3σ level. We also do bootstrap to test whether one result can be seen in the other sample. Given the number of events in sample B, we resample with replacement (each event has an equal probability of being selected) the events in sample A and measure the polarization for 100,000 times, and find that there is one time in which the PF is lower than measured from the data in sample B, suggesting that the time variation is detected at a significance of 4.4σ. Alternatively, resampling sample B with the number of events in sample A, there are 299 times in which the PF is higher than measured in sample A, corresponding to a significance of 3σ. Considering that sample A has 3,969 events and sample B has 7,671 events, the second approach is more appropriate and adopted. To conclude, the two independent means both suggest that a decrease is evident at a 3σ level.

Background and possible systematics. The measured X-ray count rate in the 3.0–4.5 keV band when observing the Crab and background regions is shown in Extended Data Fig. 5. As one can see, there is no obvious change of the background rate after the glitch. If a PF change with a factor of nearly three is caused by a change of background rate, the background fraction is required to vary from 10% to 70%, which is certainly not observed. When observing the background regions, the satellite is operated in the magnetic control mode and the star track is usually not valid. Thus, we can only calculate the polarization of background in the detector plane rather than in the sky plane. In fact, instrument rotation during observations will lower the background modulation, if any, on the sky plane. The total number of photons in 3.0–4.5 keV collected in the background regions after particle discrimination is only 680. The PF in the background data can not be detected, with a 90% upper limit of 0.28, which, along with a flux fraction of 10%, is insufficient to account for the observed change in PF. The residual modulation of this type of detector is below 1% averaged over the whole detector plane[38]. For the PolarLight flight model, owing to a tight schedule, we did not calibrate its residual modulation because the statistical limit is well above the systematic limit. The gain uniformity test with a ^{55}Fe source measured PF $= 0.009^{+0.007}_{-0.009}$ (90%) with about 2.3×10^4 photons. Thus, the residual modulation of the detector must be low, and it should be a constant effect and can not account for the variation. Another possibility of systematics is that the modulation factor was misestimated after the glitch. This is possible if the gain calibration is not accurate. As mentioned above, the uncertainty of gain calibration is roughly 1%, or less than 5% conservatively. This yields an uncertainty of 5% in μ, which is not sufficient to account for the observed variation in PF. Also, the modulation factor is found to vary no more than 4% at 3.74 keV (measured with the Al crystal) in a gain range that covers the observed range in the orbit. This, again, is unable to account for the observed change in PF. We want to emphasize that all these possible systematics or background effects will have the same effect on both on-pulse and off-pulse results, and can thus be ruled out.

Data availability
The datasets generated and analysed in this study are available from the corresponding author on reasonable request.

References
1. Novick, R., Weisskopf, M. C., Berthelsdorf, R., Linke, R. & Wolff, R. S. Detection of X-ray polarization of the Crab nebula. *Astrophys. J.* **174**, L1 (1972).
2. Weisskopf, M. C. et al. Measurement of the X-ray polarization of the Crab nebula. *Astrophys. J.* **208**, L125–L128 (1976).
3. Weisskopf, M. C., Silver, E. H., Kestenbaum, H. L., Long, K. S. & Novick, R. A precision measurement of the X-ray polarization of the Crab nebula without pulsar contamination. *Astrophys. J.* **220**, L117–L121 (1978).
4. Silver, E. H. et al. Search for X-ray polarization in the Crab pulsar. *Astrophys. J.* **225**, 221–225 (1978).
5. Dyks, J., Harding, A. K. & Rudak, B. Relativistic effects and polarization in three high-energy pulsar models. *Astrophys. J.* **606**, 1125–1142 (2004).
6. Takata, J. & Chang, H. K. et al. Pulse profiles, spectra, and polarization characteristics of nonthermal emissions from the Crab-like pulsars. *Astrophys. J.* **670**, 677–692 (2007).
7. Harding, A. K. & Kalapotharakos, C. Multiwavelength polarization of rotation-powered pulsars. *Astrophys. J.* **840**, 73 (2017).
8. Bucciantini, N., Bandiera, R., Olmi, B. & Del Zanna, L. Modeling the effect of small-scale magnetic turbulence on the X-ray properties of pulsar wind nebulae. *Mon. Not. R. Astron. Soc.* **470**, 4066–4074 (2017).
9. Feng, H. et al. PolarLight: a CubeSat X-ray polarimeter based on the gas pixel detector. *Exp. Astron.* **47**, 225–243 (2019).
10. Costa, E. et al. An efficient photoelectric X-ray polarimeter for the study of black holes and neutron stars. *Nature* **411**, 662–665 (2001).
11. Bellazzini, R. et al. A photoelectric polarimeter based on a micropattern gas detector for X-ray astronomy. *Nucl. Instrum. Methods Phys. Res. A* **510**, 176–184 (2003).
12. Cheng, K. S., Ho, C. & Ruderman, M. Energetic radiation from rapidly spinning pulsars. II. Vela and Crab. *Astrophys. J.* **300**, 522–539 (1986).
13. Muslimov, A. G. & A. K., Harding High-altitude particle acceleration and radiation in pulsar slot gaps. *Astrophys. J.* **606**, 1143–1153 (2004).
14. Kalapotharakos, C., Kazanas, D., Harding, A. & Contopoulos, I. Toward a realistic pulsar magnetosphere. *Astrophys. J.* **749**, 2 (2012).
15. Baym, G., Pethick, C. & Pines, D. Superfluidity in neutron stars. *Nature* **224**, 673–674 (1969).
16. Anderson, P. W. & Itoh, N. Pulsar glitches and restlessness as a hard superfluidity phenomenon. *Nature* **256**, 25–27 (1975).
17. Alpar, M. A., Chau, H. F., Cheng, K. S. & Pines, D. Postglitch relaxation of the Vela pulsar after its first eight large glitches: a reevaluation with the vortex creep model. *Astrophys. J.* **409**, 345–359 (1993).
18. Kallman, T. Astrophysical motivation for X-ray polarimetry. *Adv. Space Res.* **34**, 2673–2677 (2004).
19. Soffitta, P. et al. XIPE: the X-ray imaging polarimetry explorer. *Exp. Astron.* **36**, 523–567 (2013).
20. Bellazzini, R. et al. Photoelectric X-ray polarimetry with gas pixel detectors. *Nucl. Instrum. Methods Phys. Res. A* **720**, 173–177 (2013).
21. Kislat, F., Clark, B., Beilicke, M. & Krawczynski, H. Analyzing the data from X-ray polarimeters with Stokes parameters. *Astropart. Phys.* **68**, 45–51 (2015).
22. Shaw, B. et al. A glitch in the Crab pulsar (PSR B0531+21). *Astronomer's Telegram* **12957**, 1 (2019).
23. Thomas, R. M. & Fenton, K. B. The pulsed fraction of X-rays from the Crab nebula. In *International Cosmic Ray Conference* Vol. 1 (ed. Pinkau, K.) 188–193 (Max Planck Institute for Extraterrestrial Physics, 1975).
24. Ruderman, M., Zhu, T. & Chen, K. Neutron star magnetic field evolution, crust movement, and glitches. *Astrophys. J.* **492**, 267–280 (1998).
25. Palfreyman, J., Dickey, J. M., Hotan, A., Ellingsen, S. & van Straten, W. Alteration of the magnetosphere of the Vela pulsar during a glitch. *Nature* **556**, 219–222 (2018).
26. Wong, T., Backer, D. C. & Lyne, A. G. Observations of a series of six recent glitches in the Crab pulsar. *Astrophys. J.* **548**, 447–459 (2001).
27. Alpar, M. A., Chau, H. F., Cheng, K. S. & Pines, D. Postglitch relaxation of the Crab pulsar after its first four major glitches: the combined effects of crust cracking, formation of vortex depletion region and vortex creep. *Astrophys. J.* **459**, 706–716 (1996).
28. Weisskopf, M. C. et al. The Imaging X-ray Polarimetry Explorer (IXPE). In *Society of Photo-Optical Instrumentation Engineers Conference Series* Vol. 9905 (eds den Herder, J.-W. A. et al.) 990517 (SPIE, 2016).
29. Zhang, S. et al. The enhanced X-ray timing and polarimetry mission—eXTP. *Sci. China Phys. Mech. Astron.* **62**, 29502 (2019).
30. Jeffreys, H. *The Theory of Probability* 3rd edn (Oxford Classic Texts in the Physical Sciences, Oxford Univ. Press, 1961).
31. Kirsch, M. G. et al. Crab: the standard X-ray candle with all (modern) X-ray satellites. In *Society of Photo-Optical Instrumentation Engineers Conference Series* Vol. 5898 (Siegmund, O. H. W.) 589803 (SPIE, 2005).
32. Muleri, F. et al. Spectral and polarimetric characterization of the gas pixel detector filled with dimethyl ether. *Nucl. Instrum. Methods Phys. Res. Sect. A* **620**, 285–293 (2010).
33. Folkner, W. M., Williams, J. G., Boggs, J. G., Park, R. S. & Kuchynka, P. The planetary and lunar ephemerides DE430 and DE431. *Interplanet. Netw. Prog. Rep.* **42**, 196 (2014).
34. Lyne, A. G., Pritchard, R. S. & Graham Smith, F. 23 years of Crab pulsar rotational history. *Mon. Not. R. Astron. Soc.* **265**, 1003–1012 (1993).
35. Mikhalev, V. Pitfalls of statistics-limited X-ray polarization analysis. *Astron. Astrophys.* **615**, A54 (2018).
36. Maier, D., Tenzer, C. & Santangelo, A. Point and interval estimation on the degree and the angle of polarization: a Bayesian approach. *Publ. Astron. Soc. Pac.* **126**, 459–468 (2014).
37. Chauvin, M. et al. The PoGO+ view on Crab off-pulse hard X-ray polarization. *Mon. Not. R. Astron. Soc.* **477**, L45–L49 (2018).
38. Li, H. et al. Assembly and test of the gas pixel detector for X-ray polarimetry. *Nucl. Instrum. Methods Phys. Res. A* **804**, 155–162 (2015).

Author contributions
H.F. is the principal investigator of PolarLight and led the project. H.L. and X.L. conducted the daily operation of the CubeSat and had a major contribution to the data

Competing interests

The authors declare no competing interests.

Additional information

Extended data is available for this paper at https://doi.org/10.1038/s41550-020-1088-1.

Correspondence and requests for materials should be addressed to H.F.

Peer review information *Nature Astronomy* thanks Mozsi Kiss, Andrea Santangelo and the other, anonymous, reviewer(s) for their contribution to the peer review of this work.

Reprints and permissions information is available at www.nature.com/reprints.

Publisher's note Springer Nature remains neutral with regard to jurisdictional claims in published maps and institutional affiliations.
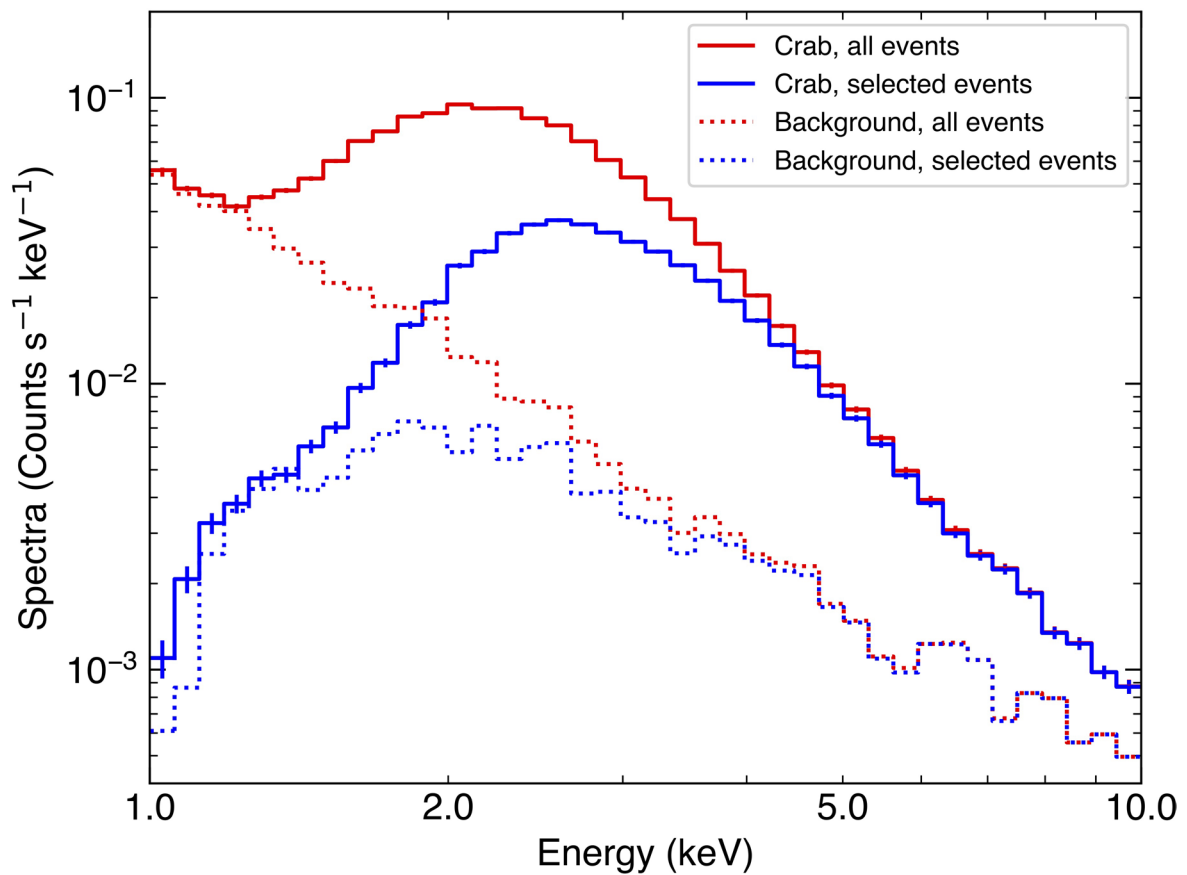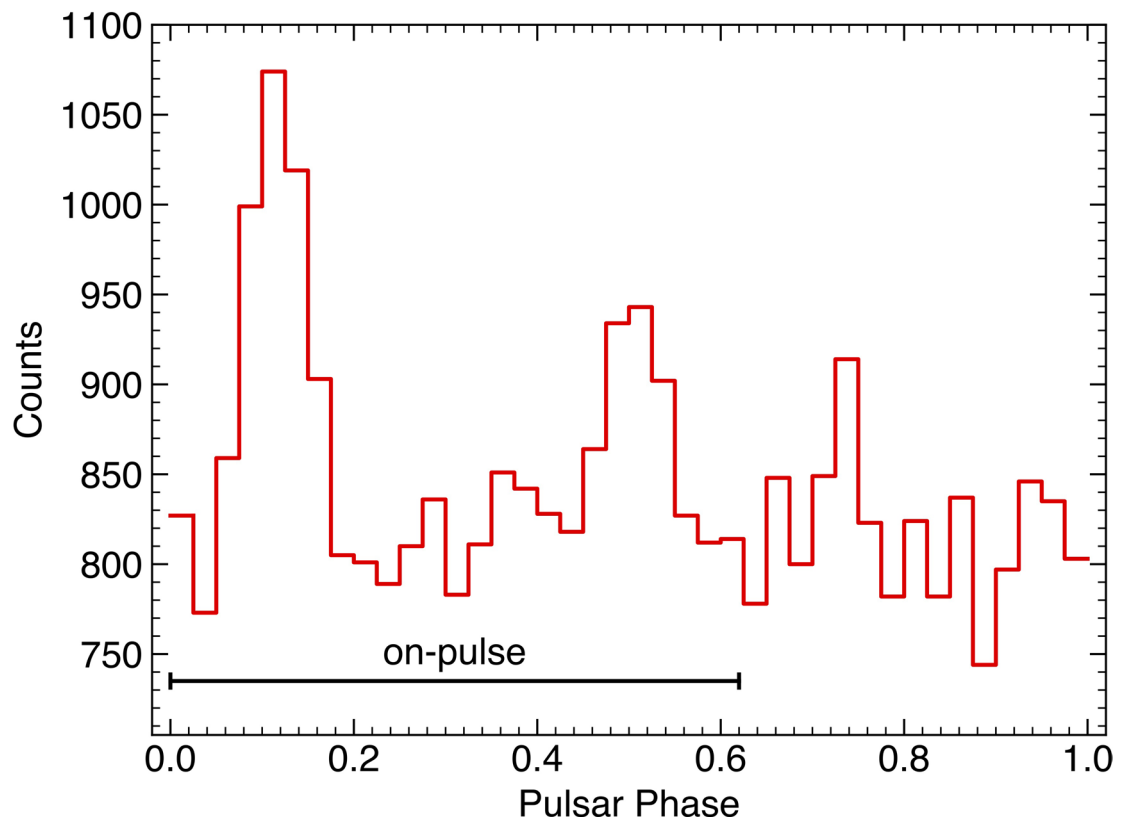
Extended Data Fig. 1 | Energy spectra measured with PolarLight. The solid curves are for the Crab and the dotted are for the background. The background spectra are obtained by observing source-free regions. The red spectra are constructed using all x-ray events passing from particle discrimination and the blue ones consist of events used for polarimetry (with one more criterion on the number of fired pixels). Errors of 1σ are shown on the two Crab spectra. We note that the background events shown in the plot are mainly due to charged particles but can not be distinguished by particle discrimination. A discussion on the time variation and modulation of the background can be found in Methods.
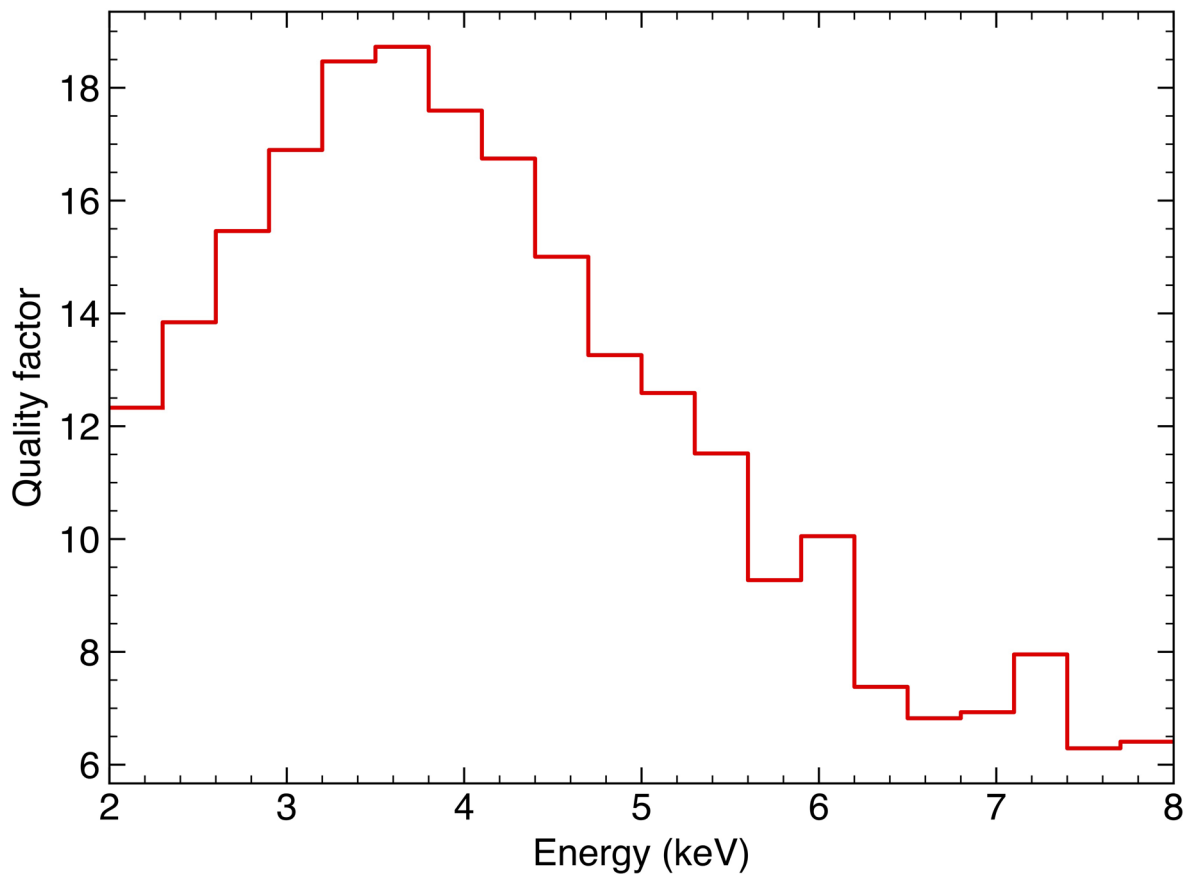
Extended Data Fig. 2 | Quality factor as a function of energy. Polarization quality factor of PolarLight when observing the Crab.

Extended Data Fig. 3 | Pulse profile of the Crab pulsar. Folded pulse profile of the Crab pulsar measured with PolarLight in the energy band of 3.0-4.5 keV. The on-pulse phase interval is indicated by the horizontal bar.
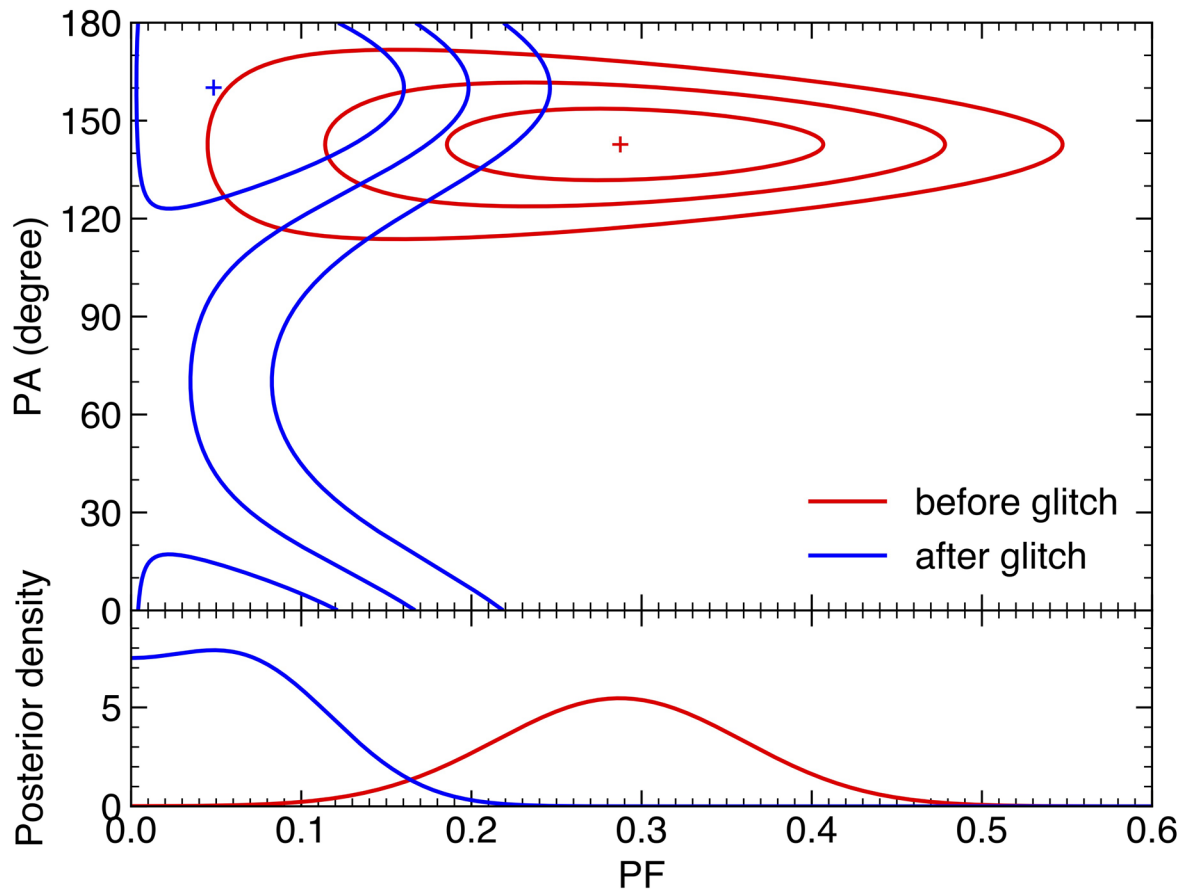
Extended Data Fig. 4 | Posterior distributions. Top: posterior distributions of PF and PA with data before the glitch (red) or data within 100 days after the glitch (blue). Bottom: posterior distribution of PF (marginalized over PA). Each measurement is not consistent with the other at a 3σ level, and this conclusion is valid if one chooses any date from 30 days to 100 days after the glitch.
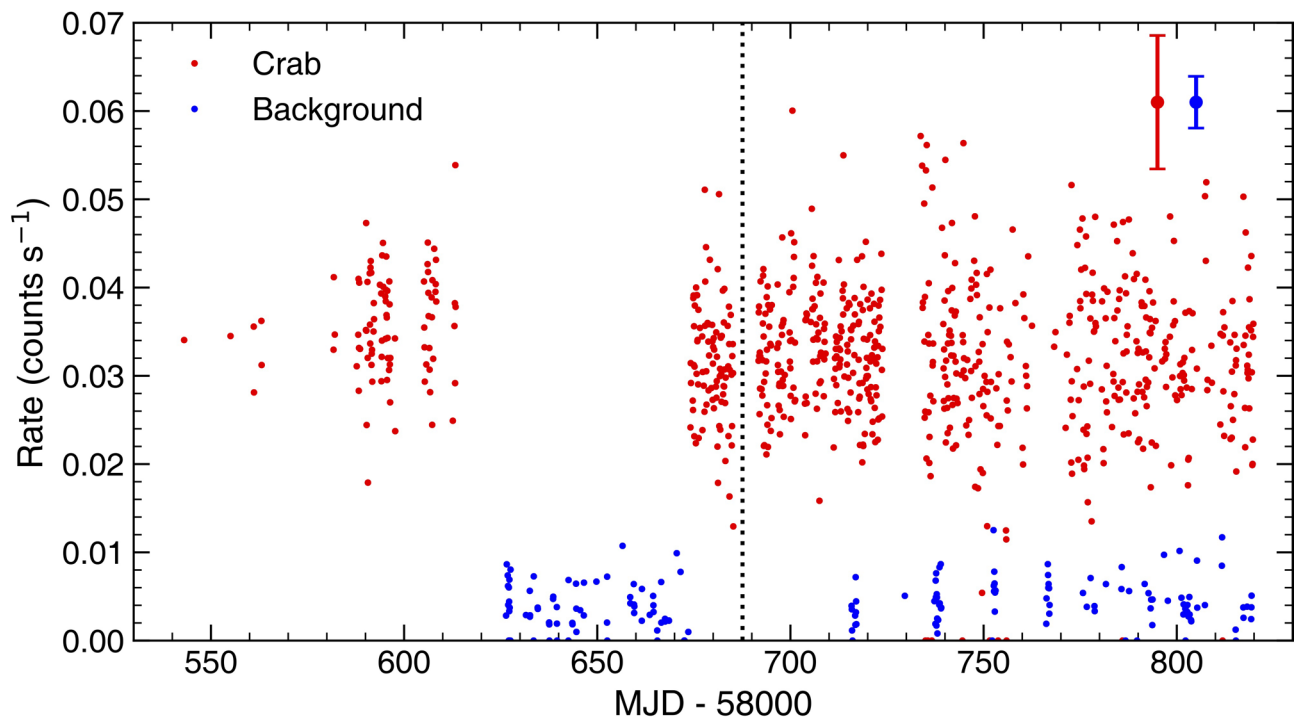
Extended Data Fig. 5 | Lightcurves for the Crab and background. 3.0–4.5 keV lightcurves measured with PolarLight when observing the Crab and background regions. The bars show typical errors. Each point is the count rate averaged in a continuous exposure, which varies and has a typical duration of 15 minutes. The gap in the Crab data from MJD 58620 to 58670 (early May to early July, 2019) is due to a small angular separation to the Sun, which precludes observations in this period.